

Structural origin of the high-voltage instability of lithium cobalt oxide

Jianyuan Li^{1,2,6}, Cong Lin^{1,2,6}, Mouyi Weng¹, Yi Qiu², Pohua Chen², Kai Yang¹, Weiyuan Huang¹, Yuexian Hong², Jian Li², Mingjian Zhang¹, Cheng Dong¹, Wenguang Zhao¹, Zhi Xu³, Xi Wang⁴, Kang Xu¹, Junliang Sun¹ and Feng Pan¹

Layered lithium cobalt oxide (LiCoO₂, LCO) is the most successful commercial cathode material in lithium-ion batteries. However, its notable structural instability at potentials higher than 4.35 V (versus Li/Li⁺) constitutes the major barrier to accessing its theoretical capacity of 274 mAh g⁻¹. Although a few high-voltage LCO (H-LCO) materials have been discovered and commercialized, the structural origin of their stability has remained difficult to identify. Here, using a three-dimensional continuous rotation electron diffraction method assisted by auxiliary high-resolution transmission electron microscopy, we investigate the structural differences at the atomistic level between two commercial LCO materials: a normal LCO (N-LCO) and a H-LCO. These powerful tools reveal that the curvature of the cobalt oxide layers occurring near the surface dictates the structural stability of the material at high potentials and, in turn, the electrochemical performances. Backed up by theoretical calculations, this atomistic understanding of the structure-performance relationship for layered LCO materials provides useful guidelines for future design of new cathode materials with superior structural stability at high voltages.

he performance of lithium-ion batteries (LIBs) is dictated by the capability and reversibility of their electrodes for accommodating Li⁺ (refs. ^{1,2}). In particular, the structural stability of cathodes at high potentials constitutes the major barrier that restricts their practical power and energy densities^{3,4}. A typical example is the layered lithium cobalt oxide (LiCoO2, LCO), which served as the very first LIB cathode in the 1990s and remains competitive today against other cathode chemistries due to its easy preparation, excellent conductivity and high energy density⁵. However, its structural instability at potentials higher than 4.35 V (versus Li/Li+) prevents access to its theoretical capacity of 274 mAh g⁻¹. At these high voltages, the layered structure collapses when most intercalated Li⁺ are removed. This has been shown by in-situ powder X-ray diffraction (PXRD) and solid-state nuclear magnetic resonance (SSNMR) techniques^{6,7}. As a result, only about half of the intercalated Li⁺ in the LCO structure can be reversibly used, leading to a capacity of ~140 mAh g⁻¹. To stabilize LCO at higher voltages, numerous strategies have been exploited8,9, among which protective treatments, such as surface doping and coating, have exhibited tangible advantages against deterioration of the cathode/electrolyte $interface ^{10,11}. \\$

A few high-voltage LCO (H-LCO) materials have recently been commercialized. Representative materials include the co-doping of LCO with La and Al, achieving 182.4 mAh g⁻¹ (4.5 V versus Li/Li⁺, 0.1C, 50 cycles), or with Mg, Al and Ti, achieving 174 mAh g⁻¹ (4.6 V versus Li/Li⁺, 0.5C, 100 cycles) or 169.9 mAh g⁻¹ (4.6 V versus Li/Li⁺, 0.1C, 200 cycles)¹¹⁻¹³. However, the exact structural role of these trace elements in stabilizing LCO layers is still elusive. Although various in-situ tools, such as PXRD, SSNMR and X-ray absorption spectroscopy, have been applied to monitor their structural

evolution, these techniques give average structural information on the microscale. This is insufficient to discern the exact structural origin of the H-LCO layer stability at high potentials^{6–15}.

A powerful nanoscale probe is available from the many emerging techniques developed on the basis of transmission electron microscopy (TEM). Spherical aberration-corrected TEM, for example, has already been widely used to provide atomic information on LIB materials in real space 16,17, but three-dimensional electron diffraction (3D ED) in reciprocal space has been employed less in LIB fields 18-20. This technique offers two main advantages: fast and automated structural information on a large length scale (single crystallite), which is otherwise unavailable from conventional two-dimensional selected-area ED, and an easier interpretation of local structural disorder or twin information than PXRD 21. One of the advanced 3D ED techniques, continuous rotation electron diffraction (cRED), has already proved its unique capability in characterizing other nanomaterials 22,23, but so far has not been applied to LIB materials.

Here, we use cRED as the main characterization tool to study the structures of two commercial LCO cathodes: a normal LCO (N-LCO) and a H-LCO, under different cut-off voltages. We chose commercial rather than laboratory-synthesized LCOs to be able to directly relate the understanding achieved to practical applications. We study the performance and macroscopic structural evolution of these two materials at high potentials, and then inspect their microstructures via combining cRED and high-resolution TEM (HRTEM) images. We find that the structural stability is correlated to the flatness of the cobalt oxide layers near the surface region, a factor not previously considered. This observation is corroborated by theoretical calculations.

¹School of Advanced Materials, Peking University, Shenzhen Graduate School, Shenzhen, China. ²College of Chemistry and Molecular Engineering, Peking University, Beijing, China. ³Beijing National Laboratory for Condensed Matter Physics, Institute of Physics, Chinese Academy of Sciences, Beijing, China. ⁴Key Laboratory of Luminescence and Optical Information, Ministry of Education, School of Science, Beijing Jiaotong University, Beijing, China. ⁵Battery Science Branch, US Army Research Laboratory, Adelphi, MA, USA. ⁶These authors contributed equally: Jianyuan Li, Cong Lin. [™]e-mail: lincong@pku.edu.cn; conrad.k.xu.civ@mail.mil; junliang.sun@pku.edu.cn; panfeng@pkusz.edu.cn

ARTICLES NATURE NANOTECHNOLOGY

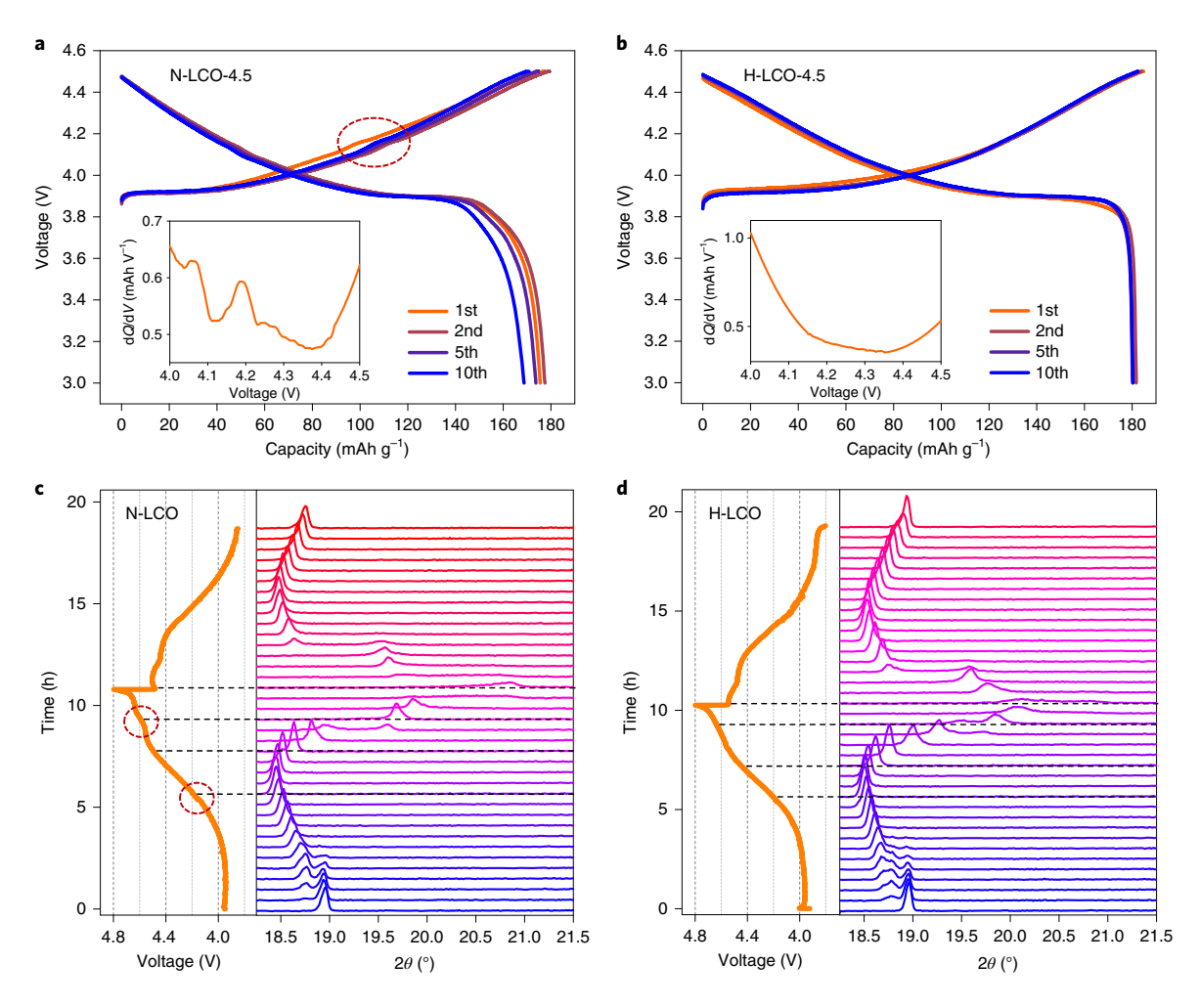


Fig. 1 | Electrochemical and in-situ PXRD characterizations of N-LCO and H-LCO during their first charge-discharge process. **a**, Charge-discharge voltage profiles of N-LCO at 0.1C. **b**, Charge-discharge voltage profiles of H-LCO at 0.1C. **c**, The voltage profile and corresponding in-situ PXRD evolution of N-LCO. **d**, The voltage profile and corresponding in-situ PXRD evolution of H-LCO. The order-disorder transition in **a** is highlighted in the orange dashed circle. The insets in **a** and **b** are the corresponding dQ/dV curves of the first charge process. The obvious transition in **c** is highlighted in the red dashed circle.

Electrochemical performance and structural evolution by in-situ PXRD

Both LCO materials exhibit round morphology with obvious fragments in pristine N-LCO (N-LCO-P, Supplementary Fig. 1a,b). Consistent with previous reports^{11,12}, trace Mg, Al and Ti are detected in pristine H-LCO (H-LCO-P, Supplementary Fig. 1d,f,h), which are, however, also observed in N-LCO-P (Supplementary Fig. 1c,e,g). Quantitative analysis on N-LCO-P and H-LCO-P yields Mg/Al/Ti/Co atom ratios of ~1.028/1.258/0.264/100 and ~0.677/1.184/0.209/100, respectively (Supplementary Table 1). Synchrotron PXRD refinements indicate that both pristine materials possess the layered structure (Supplementary Fig. 2d) with high crystallinity and purity, but no structural differences are acquired except the slightly larger interlamellar spacing from the little, sharper (003) peak in H-LCO-P (Supplementary Fig. 2a-c)^{5,13}. Overall, no obvious difference exists between the two pristine LCOs.

Their electrochemical performances were evaluated by half-cells cycled at 0.1C with different cut-off voltages (4.2 V, 4.5 V, 4.6 V and 4.8 V versus Li/Li⁺; the samples are denoted as N-LCO-n and H-LCO-n, respectively) (Fig. 1a,b and Supplementary Fig. 3). In accordance with previous reports^{7-9,24,25}, N-LCO experiences a series of structural transformations during charge with obvious capacity decay, which, however, become rare and more sluggish

in H-LCO according to the distinct dQ/dV curves (insets in Fig. 1 and Supplementary Fig. 3) with better reversibility (Supplementary Note 1). Overall, the electrochemical results verify the superior performance of H-LCO over N-LCO, but the underlying structural origin remains ill defined.

To directly correlate the structure evolution with the state-ofcharge, the first electrochemical cycles of N-LCO and H-LCO were carried out using in-situ PXRD (Fig. 1c,d), which was combined with the dQ/dV results to provide intrinsic details (Supplementary Fig. 4 and Supplementary Note 2). Briefly, N-LCO experiences successive phases of H1, H2, M1 and H3 during charging to 4.5 V (refs. 7-9), and H1-3 and O1 when deep charged with large interlamellar spacing changes (Supplementary Table 2)24,25. The poorly reversible H3-(H1-3) transition from the H1-3 instability^{11,12,24-27} accompanied by deep lithiation, Co3+ oxidization and possible O2oxidization with CO2 release from the differential electrochemical mass spectroscopy (DEMS, Supplementary Fig. 5)11,28, is responsible for eventual structural collapse during the N-LCO cycling process. In stark contrast, M1, H3 and O1, as well as CO2 release, are entirely absent in H-LCO when charged to 4.8 V, with the final H1-3 observed to become amorphous, and the evolution is also much more sluggish with smaller interlamellar spacing changes. These results agree with the electrochemical performance. However, due

ARTICLES

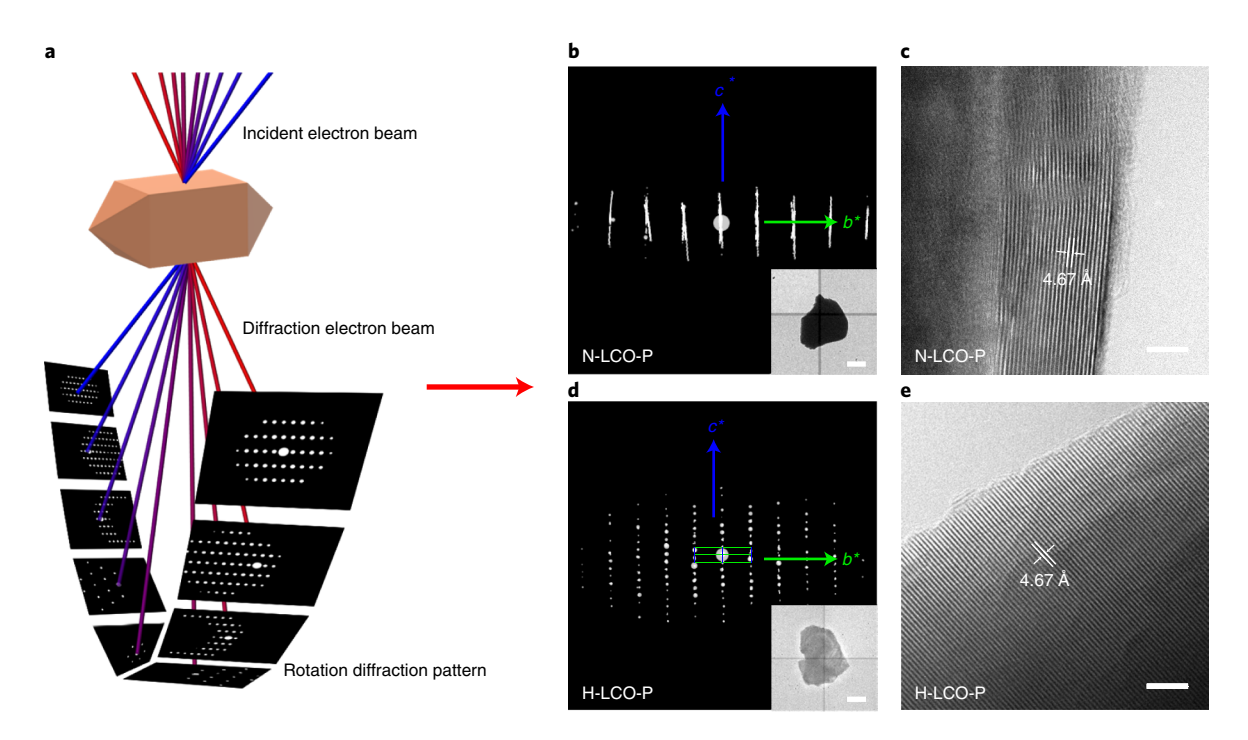


Fig. 2 | **cRED** schematic and the combined **cRED** and **HRTEM** characterizations of pristine **LCOs. a**, Schematic of the data collection process of cRED. **b,d**, The reciprocal lattice along the *a*' axis of N-LCO-P (**b**) and H-LCO-P (**d**). **c,e**, HRTEM image of N-LCO-P (**c**) and H-LCO-P (**e**). The attached 'P' in N-LCO-P and H-LCO-P represents 'pristine'. The insets in **b** (scale bar, 500 nm) and **d** (scale bar, 1μm) are the corresponding particles for cRED. Scale bar in **c,e**, 5 nm.

to the relatively small structural variation below 4.5 V, and the M1 presence in some H-LCO materials^{11,12}, the transitions at low voltages are thought to have little effect on LCO stability. Unfortunately, the origin of the excellent H-LCO structural stability remains unclear from these macroscopic characterizations alone.

Structural origin on the atomistic level

Since the electrochemical performance hardly correlates with the two LCO materials possessing almost identical components and structures, the cRED technique was applied. Only one sample particle participated and was continuously rotated with the TEM holder to produce electron diffraction from different directions (Fig. 2a)^{22,23}, which is more sensitive than PXRD to the local atomic environment due to its nanoscale features. To ensure accuracy and reliability, another TEM-based technique, that is, HRTEM, was also applied as an auxiliary.

To validate the feasibility, preliminary cRED experiments were conducted on H-LCO-P (Supplementary Video 1). The 3D reciprocal lattice reconstructed from cRED data shows discrete and well-shaped reflections with an identifiable unit cell (Supplementary Fig. 6), suggesting the high and single crystallinity while revealing flat stacking of the cobalt oxide layers due to the regular reflection arrangement along the c axis. Such results are in excellent agreement with the HRTEM image (Supplementary Fig. 2e), where the lattice fringes with ~4.68-Å spacing are recognized as the (003) planes and ascribed to the cobalt oxide layers. Therefore, such fringes in the HRTEM directly reflect the stacking and flatness information of the cobalt oxide layers from real space, while cRED provides such knowledge from reciprocal space.

The pristine LCOs were then analysed by cRED. For N-LCO-P, although a reconstructed discrete reciprocal lattice similar to the preliminary experiment can be obtained, streaked reflections along the c^* axis are also observed (Fig. 2b and Supplementary Video 2). Such results are not due to the twinning of the rhombus lattice, but rather arise from the disorder of the cobalt oxide layers along the

c* axis, as discussed above, which brings difficulties in determining the unit cell. Meanwhile, in the vicinity of the surface, HRTEM images reveal obvious curve and dislocation of the cobalt oxide lavers (Fig. 2c and Supplementary Fig. 7a), which is consistent with cRED. The occurrence of such curved layers in N-LCO-P was later quantified from cRED results, showing a large disordered ratio with streaked reflections (Supplementary Fig. 12). It is worth mentioning that similar curved fringes of LCO have already been observed in the literature^{12,29}, but, unfortunately, they are discarded as 'bad data' and do not attract the attention they deserve. Such curved layers are especially common in various two-dimensional materials, such as single-layer graphene and zeolite with ripples or wrinkling^{30,31}, van der Waals crystals of hexagonal BN and MoS2, where the curvature is induced by external force^{32,33}. As for H-LCO-P, although streaked reflections are also observed, this occurs less frequently. The typical discrete reciprocal lattice from cRED and flat lattice fringes from HRTEM indicate the absence of any evident curvature in H-LCO-P layers (Fig. 2d,e and Supplementary Fig. 8a). Thus, combined cRED and HRTEM reveal a pronounced difference between the two pristine LCOs in the flatness of the cobalt oxide layers, which is otherwise unavailable via PXRD.

Since direct HRTEM only reflects a specific thin area, especially near the surface region, focused-ion beam (FIB) milling was employed to complement HRTEM for simultaneous imaging of both the surface and the interior (Supplementary Fig. 9). N-LCO-P possesses obvious curved fringes in its near-surface region but relatively flat ones in its interior, while H-LCO-P exhibits flat fringes in both the surface and interior. These observations suggest that the streaked reflections in cRED mainly come from the curved cobalt oxide layers in the near-surface region, indicating the high sensitivity of cRED towards the minuscule variations occurring in local structures. Although the surface curvature only occupies a very small proportion compared with the vast interior of an individual particle, such surface irregularity plays the critical role in determining the LCO electrochemical stability at high potentials, because

ARTICLES NATURE NANOTECHNOLOGY

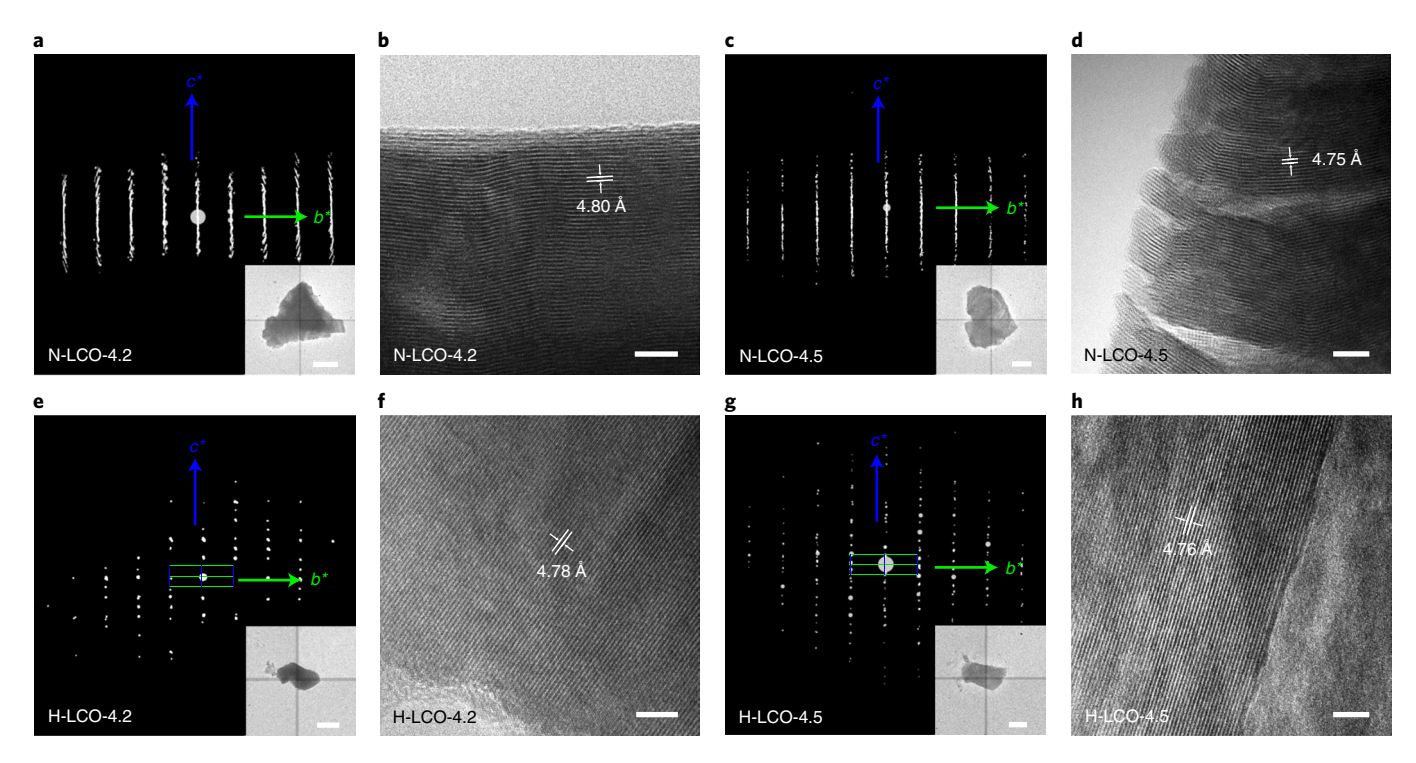


Fig. 3 | Combined cRED and **HRTEM** characterizations of charged **LCOs. a,c,e,g,** The reciprocal lattice viewed along the *a*' axis of N-LCO-4.2 (**a**), N-LCO-4.5 (**c**), H-LCO-4.2 (**e**) and H-LCO-4.5 (**g**). **b,d,f,h**, HRTEM images of N-LCO-4.2 (**b**), N-LCO-4.5 (**d**), H-LCO-4.2 (**f**) and H-LCO-4.5 (**h**). The attached numbers after N-LCO and H-LCO represent the charge voltage values. The insets in **a** (scale bar, 500 nm), **c** (scale bar, 1μm), **e** (scale bar, 500 nm) and **g** (scale bar, 500 nm) are the corresponding particles for cRED. Scale bar in **b,d,f,h**, 5 nm.

those structures in direct contact with electrolyte serve as the gate to regulate the entrance and exit of Li⁺. Therefore, such interfacial curvature is important for bulk LCO stability. This might be the fundamental reason why various modifications, such as surface doping and coating, are efficient for improving LCO cyclability^{8-12,25}. The capability of cRED for capturing such minor but critical structural information, which would otherwise be neglected using either PXRD or conventional TEM, should present a powerful tool for understanding and engineering better lattice structures.

We then applied combined cRED and HRTEM on the charged LCOs. At 4.2 V, streaked reflections are still observed in N-LCO-4.2 without an identifiable unit cell (Fig. 3a and Supplementary Video 3). This indicates the existence of more severe curvature in the cobalt oxide layers when charged, due to the enlarged disorder occurrence (Supplementary Fig. 12), thus leading to higher stress at the nanoscale (Fig. 3b and Supplementary Fig. 7b). However, H-LCO-4.2 exhibits consistently ordered reciprocal lattices and planar lattice fringes (Fig. 3e,f, Supplementary Figs. 8b and 12 and Supplementary Video 4). Although the disorder-related curved layers are observed both in N-LCO-4.2 and H-LCO-4.2, nearly all particles remain stable due to their constant capacity (Supplementary Figs. 3a,d). Increasing the charge voltage to 4.5 V uncovers notable structural differences from both cRED and HRTEM. Besides the severely streaked reflections (Supplementary Fig. 12 and Supplementary Video 5), an obvious decrease in both the reflection number and intensity is also observed for N-LCO-4.5 (Fig. 3c). This apparent departure from a flat layer structure implies rather severe disorder along the layer-stacking direction, which is further confirmed by HRTEM showing numerous disordered domains with curved fringes, dislocations and even voids in both the surface and the interior (Fig. 3d and Supplementary Figs. 7c and 9c,d). During deep charging, the removal of the massive Li+ ion changes the interlamellar spacing, while the Co3+ oxidation reduces the Co-O

lengths and alters the CoO₆ coordination status. The inherent curvature in pristine LCOs is thus dramatically intensified for both the interlayer and intralayer structures. Furthermore, the deteriorated curvature builds up increasing stress, destabilizes the layered structure with irreversible phase transitions and eventually leads to rapid capacity fading. Such curved cobalt oxide layers may also induce the oxidized On- species to release O2 due to the reduced O2- distance between adjacent layers at certain locations (Supplementary Fig. 10). H-LCO-4.5, however, maintains its layered structure, with more observations of clear reciprocal lattice (Fig. 3g, Supplementary Fig. 12 and Supplementary Video 6) and flat lattice fringes in both the surface and the interior (Fig. 3h and Supplementary Figs. 8c and 9g,h), indicating a superior structural stability with stacking of flat cobalt oxide layers that stably supply larger capacity from the available accommodation of Li+. Further increasing the voltage removes more Li+ with severely deteriorated curvature, leading to catastrophic structural collapse and fragmentation of most N-LCO particles, as evidenced by the far fewer disordered reflections with lower intensity from cRED and the curve-induced broken fringes with large-scale cracks in HRTEM (Supplementary Fig. 7d-i). Although similar scenarios also appear at extreme potential in H-LCO-4.8 (Supplementary Fig. 8g-i), a regular reciprocal lattice with planar fringes is obtained in H-LCO-4.6 (Supplementary Fig. 8d-f), indicating that H-LCO is more resilient against higher voltages. Besides the extent of curvature in cobalt oxide layers, destruction of H-LCO structure with high voltages is also found to be more sluggish due to the flat layer stacking, thus contributing to its superior performance.

Meanwhile, it is noteworthy that both flat and curved cobalt oxide layers coexist in all tested LCOs, but their probability of occurrence differs obviously. For example, both ordered reciprocal lattice and flat lattice fringes can be discovered in N-LCO-4.5 at a low concentration, while the reverse is true for H-LCO-4.5

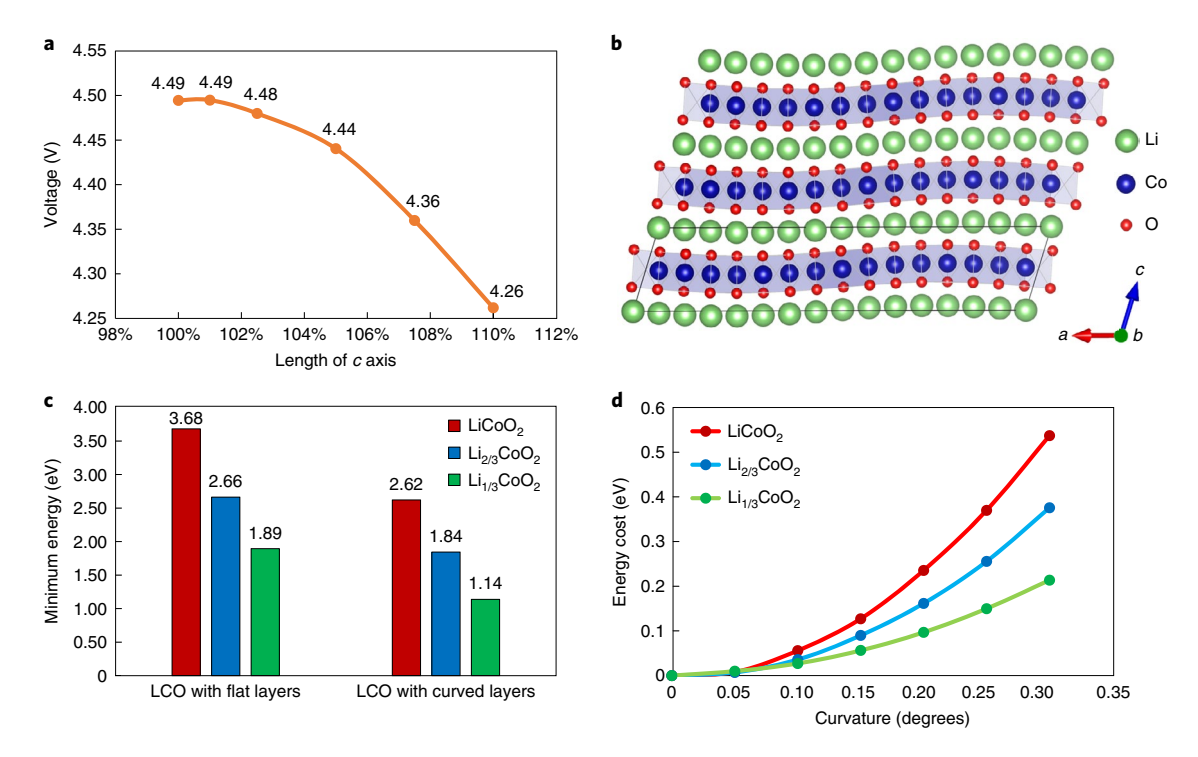


Fig. 4 | Theoretical calculations of curved LCO structure. a, The relationship between the lattice length of the *c* axis and the theoretical delithiation voltage for one Li atom from the LCO supercell. **b**, Schematic of the LCO structure with curved cobalt oxide layers viewed along the *b* axis. **c**, Minimum oxygen release energy for one oxygen atom in LCO supercells with flat and curved (curvature degree: $A = 0.25 \, \text{Å}$) cobalt oxide layers and different delithiation degrees. **d**, Energy cost for the cobalt oxide layers to curve to different curvatures with varied delithiation degrees in LCO supercells. The overall oxygen release energy for **c** is plotted in Supplementary Fig. 13. The details for supercell construction are stated in the Methods.

(Supplementary Fig. 11). Overall, as evidenced by the exact ratio of ordered occurrence from cRED (Supplementary Fig. 12), higher curvature is undoubtedly detected in N-LCO, which becomes much more serious when charged, leading to deterioration in stability and performance, while in H-LCO the occurrence of streaked reflections is basically unchanged up to high potentials. Therefore, these results validate the importance of cobalt oxide layer flatness in stabilizing LCO structure at high potentials, and this quantity is directly correlated with the degree of capacity fading upon high cut-off voltages.

Theoretical calculation of LCO structure

On the basis of the experimental results, theoretical calculations were employed to thoroughly study the influence of cobalt oxide layer curvature on LCO properties. We first explored the relationship between c-axis length and delithiation voltage by constructing a supercell with its c axis increased by 1%, 2.5%, 5%, 7.5% and 10%, to calculate the corresponding delithiation voltage for one Li atom (Fig. 4a). Clearly, the delithiation voltage decreases with increasing interlamellar spacing, indicating an expanding trend in layer curvature due to the tendency for easier delithiation.

First-principle methods were employed to quantify the influences of structural curving on the electrochemical performance and stability of LCO materials. Other periodic supercells possessing a layer curve set only in the *a* axis were built following the formula:

$$\Delta c = A \times \sin\left(\frac{a_{\text{atom}}}{a_0} \times 2\pi\right) \tag{1}$$

where a_{atom} , a_0 , A and Δc are the Co atom a coordinate, the a-axis length, the index of curvature degree and the value of deviation from the equilibrium c coordinate, respectively. Representative A values are: 0 Å (flat cobalt oxide layer), 0.125 Å (cobalt oxide layer)

with a minor degree of curvature) and 0.25 Å (cobalt oxide layer with a major degree of curvature). A typical LCO structure with curved cobalt oxide layers is illustrated in Fig. 4b. The increased Co forces along the c axis suggest decreased stability in the curved LCO structures (Supplementary Tables 3–5).

The curving in cobalt oxide layers will certainly alter the structural energy, especially for dictating oxygen release³⁴. In flat LCO structures, since all oxygen atoms are equivalent, the release energy is calculated by removing any one of them. However, in curved LCO structures, the release energy is calculated by removing every distinct oxygen atom with a different environment, to find the minimum value. Meanwhile, the degree of delithiation is also taken into consideration by constructing two partially delithiated structures: Li_{2/3}CoO₂ and Li_{1/3}CoO₂ with a major degree of curvature. The calculated results demonstrate the increase in structural instability because of the decreased oxygen release energy, which is much lower in curved Li_{2/3}CoO₂ and Li_{1/3}CoO₂ (Fig. 4c and Supplementary Fig. 13). These results suggest easier oxygen release upon deep delithiation in the presence of the cobalt oxide layer curvature, implying the instability of curved LCO structures, especially under high potentials, in accordance with cRED and HRTEM.

Finally, the structural energy of LCOs was investigated. It was found that the free energy of formation is markedly higher in curved LCOs, validating the deterioration in stability for curved cobalt oxide layers, especially at high potentials (Supplementary Fig. 14). Meanwhile, the energy cost for the cobalt oxide layers to curve was also calculated with various curvature degrees and delithiation; all the energy values are relatively small and increased with the degree of curvature, while much less energy to curve is demanded for delithiated LCO structures (Fig. 4d). These consequences indicate that the curvature in cobalt oxide layers occurs rather easily, especially upon deep delithiation, and strongly affects the structural stability, which is consistent with our experimental observations.

ARTICLES

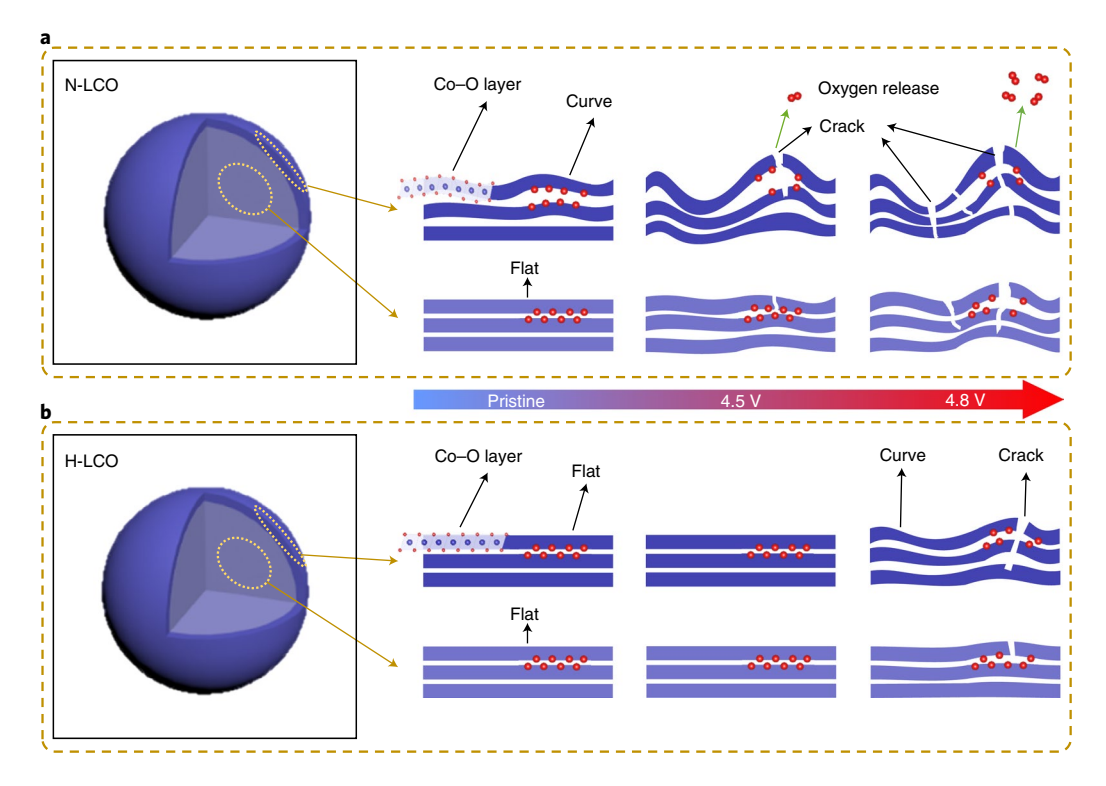


Fig. 5 | Schematic illustration of the LCO structural evolutions during charge. a, N-LCO. b, H-LCO. The flatness of the cobalt oxide layers, especially that in the near-surface region, indicating the LCO structural stability at high potentials is clearly shown.

Structural evolution during charge

From the experimental and theoretical results, the structural evolution of N-LCO and H-LCO is conjectured to be as illustrated schematically in Fig. 5. The most distinct structural difference between the two commercial LCOs is the degree of curvature of their cobalt oxide layers, especially that in the near-surface region, the probability of the emergence of which is much higher in N-LCO. Despite a certain performance improvement^{11,12}, trace doping with Mg, Al and Ti hardly alters the LCO microstructures, due to the tiny amounts present, and should not have a meaningful impact on the curvature of the cobalt oxide layers and on the overall structural stability. Since curvature is inherent, the layer flatness is speculated to be regulated by the crystal growth kinetics during synthesis. Various technological parameters, such as raw materials, temperature, atmosphere, cooling rate, etc., directly affect the cobalt oxide layer curvature generated by the layer-stacking disorder from the possible mixed stacking modes, CoO₆ distortion and/or imperfect crystal growth. Hence, LCO preparation technologies, especially those related to crystal growth kinetics for flattening the cobalt oxide layers, deserve more attention, which unfortunately is often not the case. In addition, since the cobalt oxide curvature mainly occurs in the near-surface region, there is a strong need to protect the LCO particle surface, especially that with curvature, from deep delithiation and direct contact with electrolyte, to suppress cascading structural collapse into the interior with undesired by-products that impede Li+ transport. Widely applied surface modification has been demonstrated as effective remediation to help LCO withstand high voltages to some extent⁸⁻¹², and more feasible surface approaches with this mechanism deserve thorough investigation. Therefore, the 'bad' cobalt oxide layer curvature is an indicator of structural stress and responsible for LCO structural stability in delithiation: at lower voltages, the structural variation with curved layers is reversible despite less capacity; at higher voltages, the curved structure becomes incapable of tolerating the variation, resulting in increased stress to influence the stability and capacity. Specifically, during the

charge of N-LCO with a larger layer curvature, due to continuous Li⁺ removal, the layer curvature continuously deteriorates and introduces higher structural stress and oxygen loss. These in turn result in aggravating layer curvature and further layer breakage, structure collapse and crystal fragmentation, which are more serious in the near-surface region. Thus, N-LCO performance is severely limited to lower voltages because of its structural instability at high delithiation. In contrast, the much flatter cobalt oxide layers in both the surface and interior of H-LCO suppress similar structural distortions, with a superior electrochemical performance at high voltages.

Conclusion

We have revealed the structural difference between two commercial LCO materials at the atomistic level, using a combined approach of cRED and HRTEM. The curvature of the cobalt oxide layers, especially in the vicinity of the surface, is identified as the key factor responsible for the degradation of electrochemical performances at high voltage. This is the fundamental, nanoscale origin of the surface-modification approaches reported in the literature for H-LCO cathodes. Both experimental and theoretical results show that curved LCO layers damage the material's structural stability, leading to poor electrochemical performance at high voltages. This atomistic understanding not only provides insights into LCO cathodes, but also, in a broader context, should guide the establishment of a precise structure-performance relationship for other layered oxide cathodes, such as $\text{Li}(\text{Ni}_x\text{Co}_y\text{Mn}_{1-x-y})\text{O}_2$ and $\text{Li}(\text{Ni}_{0.8}\text{Co}_{0.15}\text{Al}_{0.05})$ O₂. Future designs of layered cathode chemistries should focus on protecting the material surface via precise modifications, which can be characterized by advanced electron diffraction techniques, such as cRED.

Online content

Any methods, additional references, Nature Research reporting summaries, source data, extended data, supplementary information, acknowledgements, peer review information; details of

NATURE NANOTECHNOLOGY ARTICLES

author contributions and competing interests; and statements of data and code availability are available at https://doi.org/10.1038/s41565-021-00855-x.

Received: 15 April 2020; Accepted: 15 January 2021; Published online: 22 February 2021

References

- Liu, Y. Y., Zhu, Y. Y. & Cui, Y. Challenges and opportunities towards fast-charging battery materials. *Nat. Energy* 4, 540–550 (2019).
- Li, M., Lu, J., Chen, Z. W. & Amine, K. 30 years of lithium-ion batteries. *Adv. Mater.* 30, 1800561 (2018).
- House, R. A. et al. Superstructure control of first-cycle voltage hysteresis in oxygen-redox cathodes. Nature 577, 502–508 (2020).
- Li, W. D., Erickson, E. M. & Manthiram, A. High-nickel layered oxide cathodes for lithium-based automotive batteries. *Nat. Energy* 5, 26–34 (2020).
- Mizushima, K., Jones, P. C., Wiseman, P. J. & Goodenough, J. B. Li_xCoO₂ (0 < x ≤ 1): a new cathode material for batteries of high energy density. *Mat. Res. Bull.* 15, 783–789 (1980).
- Shimoda, K. et al. In situ NMR observation of the lithium extraction/ insertion from LiCoO₂ cathode. *Electrochim. Acta* 108, 343–349 (2013).
- Amatucci, G. G., Tarascon, J. M. & Klein, L. C. CoO₂, the end member of the Li_xCoO₂ solid solution. J. Electrochem. Soc. 143, 1114–1123 (1996).
- Wang, L. L., Chen, B. B., Ma, J., Cui, G. L. & Chen, L. Q. Reviving lithium cobalt oxide-based lithium secondary batteries-toward a higher energy density. *Chem. Soc. Rev.* 47, 6505-6602 (2018).
- Wang, X., Wang, X. Y. & Lu, Y. Y. Realizing high voltage lithium cobalt oxide in lithium-ion batteries. *Ind. Eng. Chem. Res.* 58, 10119–10139 (2019).
- Kalluri, S. et al. Surface engineering strategies of layered LiCoO₂ cathode material to realize high-energy and high-voltage Li-ion cells. Adv. Energy Mater. 7, 1601507 (2017).
- Matter, 7, 1001507 (2017).
 Zhang, J.-N. et al. Trace doping of multiple elements enables stable battery cycling of LiCoO₂ at 4.6 V. Nat. Energy 4, 594–603 (2019).
- Wang, L. L. et al. A novel bifunctional self-stabilized strategy enabling 4.6 V LiCoO₂ with excellent long-term cyclability and high-rate capacity. Adv. Sci. 6, 1900355 (2019).
- Liu, Q. et al. Approaching the capacity limit of lithium cobalt oxide in lithium ion batteries via lanthanum and aluminium doping. *Nat. Energy* 3, 936–943 (2018).
- Grey, C. P. & Dupré, N. NMR studies of cathode materials for lithium-ion rechargeable batteries. *Chem. Rev.* 104, 4493–4512 (2004).
- Tripathi, A. M., Su, W. N. & Joe-Hwang, B. In situ analytical techniques for battery interface analysis. Chem. Soc. Rev. 47, 736–851 (2018).
- Zachman, M. J., Tu, Z. Y., Choudhury, S., Archer, L. A. & Kourkoutis, L. F. Cryo-STEM mapping of solid–liquid interfaces and dendrites in lithium-metal batteries. *Nature* 560, 345–349 (2018).
- 17. Li, Y. Z. et al. Atomic structure of sensitive battery materials and interfaces revealed by cryo-electron microscopy. *Science* **358**, 506–510 (2017).

 Karakulina, O. M., Demortière, A., Dachraoui, W., Abakumov, A. M. & Hadermann, J. In situ electron diffraction tomography using a liquid-electrochemical transmission electron microscopy cell for crystal structure determination of cathode materials for Li-Ion batteries. *Nano Lett.* 18, 6286–6291 (2018).

- Hadermann, J. & Abakumov, A. M. Structure solution and refinement of metal-ion battery cathode materials using electron diffraction tomography. *Acta Crystallogr.* B75, 485–494 (2019).
- Hadermann, J. et al. Solving the structure of Li ion battery materials with precession electron diffraction: application to Li₂CoPO₄F. Chem. Mater. 23, 3540–3545 (2011).
- Willhammar, T. et al. Structure and catalytic properties of the most complex intergrown zeolite ITQ-39 determined by electron crystallography. *Nat. Chem.* 4, 188–194 (2012).
- Li, J. et al. Discovery of complex metal oxide materials by rapid phase identification and structure determination. J. Am. Chem. Soc. 141, 4990–4996 (2019).
- 23. Ma, T. Q. et al. Observation of interpenetration isomerism in covalent organic frameworks. *J. Am. Chem. Soc.* **140**, 6763–6766 (2019).
- Chen, Z. H., Lu, Z. H. & Dahn, J. R. Staging phase transition in Li_xCoO₂.
 J. Electrochem. Soc. 149, A1604–A1609 (2002).
- Lyu, Y. et al. An overview on the advances of LiCoO₂ cathodes for lithium-ion batteries. Adv. Energy Mater. 11, 2000982 (2020).
- 26. Seong, W. M., Yoon, K., Lee, M. H., Jung, S.-K. & Kang, K. Unveiling the intrinsic cycle reversibility of a LiCoO $_2$ electrode at 4.8-V cutoff voltage through subtractive surface modification for lithium-ion batteries. *Nano Lett.* **19**, 29–37 (2019).
- Hirooka, M. et al. Improvement of float charge durability for LiCoO₂ electrodes under high voltage and storage temperature by suppressing O1-phase transition. *J. Power Sources* 463, 228127 (2020).
- Zhu, Z. et al. A surface Se-substituted LiCo[O_{2-δ}Se_δ] cathode with ultrastable high-voltage cycling in pouch full-cells. Adv. Mater. 32, 2005182 (2020).
- Lu, X. et al. New insight into the atomic structure of electrochemically delithiated O3-Li_(1-x)CoO₂ (0 ≤ x ≤ 0.5) nanoparticles. Nano Lett. 12, 6192–6197 (2012).
- Fasolino, A., Los, J. H. & Katsnelson, M. I. Intrinsic ripples in graphene. Nat. Mater. 6, 858–861 (2007).
- Kumar, P., Agrawal, K. V., Tsapatsis, M. & Mkhoyan, K. A. Quantification of thickness and wrinkling of exfoliated two-dimensional zeolite nanosheet. *Nat. Commun.* 6, 7128 (2015).
- Rooney, A. P. et al. Anomalous twin boundaries in two dimensional materials. *Nat. Commun.* 9, 3597 (2018).
- 33. Tang, D. M. et al. Nanomechanical cleavage of molybdenum disulphide atomic layers. *Nat. Commun.* 5, 3631 (2014).
- Zheng, J. et al. Tuning of thermal stability in layered Li(Ni_xMn_yCo_z)O₂.
 J. Am. Chem. Soc. 138, 13326–13334 (2016).

Publisher's note Springer Nature remains neutral with regard to jurisdictional claims in published maps and institutional affiliations.

 $\ensuremath{\texttt{©}}$ The Author(s), under exclusive licence to Springer Nature Limited 2021

ARTICLES NATURE NANOTECHNOLOGY

Methods

Material characterization. N-LCO and H-LCO were purchased from Tianjin B&M Science and Technology and Sichuan Kaiyuan Huineng Science and Technology, respectively, and used without further treatment. The particle morphology of the commercial N-LCO and H-LCO were examined by a ZEISS SUPRA 55 field-emission scanning electron microscope (SEM) with an accelerating voltage of 5 kV. For characterizing the constituent elements of N-LCO and H-LCO, qualitative analyses were conducted on an Oxford X-Max 20 energy-dispersive spectrometer (EDS) and an ESCALAB 250Xi X-ray photoelectron spectrometer (XPS), while the quantitative analyses were performed on a HORIBA JOBINYVON JY2000-2 inductively coupled plasma-atomic emission spectrometer (ICP-AES). The synchrotron PXRD data for structural refinement of N-LCO-P and H-LCO-P were collected by National Synchrotron Light Source II (NSLS-II) (λ = 0.18545 Å) at Brookhaven National Laboratory with the powder sample sealed in a Kapton tube. Then, structure refinement against the synchrotron PXRD data was performed using the TOPAS v.5.0 software (Brucker AXS)35.

Electrode preparation and electrochemical methods. The composite slurry for the electrochemical characterization was prepared by blending and grinding 70 wt% N-LCO or H-LCO as the active material and 20 wt% poly(vinylidenefluoride) as the binder in a mortar, which were later stirred with 10 wt% Super P as the conductive additive in N-methyl-2-pyrrolidone (NMP) solvent for 12 h. The Al foil was then coated by the slurry and dried at 110 °C under vacuum for 12h, and was later cut into cathode electrodes with a diameter of 10 mm. Typically, the loading mass of the active material for each electrode was ~1 mg. The cathode electrode was subsequently assembled into the CR2032-type coin cell in an argon-filled glovebox with water and oxygen content below 0.1 ppm, inside which the lithium metal foil, the polypropylene film (Celgard 2400) and the 1 M LiPF₆ solution containing ethylene carbonate (EC), dimethyl carbonate (DMC) and diethyl carbonate (DEC) with a volume ratio of 1:1:1 were employed as the anode, the separator and the electrolyte, respectively. The galvanostatic charge/ discharge characterization was conducted on a LAND CT3001B battery test system in the voltage range 3.0-4.8 V with a current rate of 0.1C (1C=274 mAh g⁻¹) and ten cycles at room temperature. The dQ/dV curve was later obtained from the differential of the first charge profile.

In-situ PXRD characterization. The cathode electrode for the in-situ PXRD test was prepared by blending and grinding 70 wt% N-LCO or H-LCO as the active material, 20 wt% polytetrafluoroethylene (dissolved in isopropanol with a 5 wt% mass fraction) as the binder and 10 wt% acetylene black as the conductive additive, with isopropanol in a mortar. The composite then became a rubber-like paste after the volatilization of isopropanol and was quickly shaped into a large slice with a thickness of \sim 20 μm using a roll squeezer, and was afterwards cut into small slices with a size of ~8 mm × 8 mm and dried at 110 °C under vacuum for 12 h. The obtained cathode slice was subsequently assembled into the customized stainless-steel in-situ cell (Beijing SciStar Technology) possessing an X-ray 'transparent' beryllium window in an argon-filled glovebox, with water and oxygen content below 0.1 ppm, inside which the lithium metal foil, the polypropylene film (Celgard 2400) and the 1 M LiPF₆ solution containing EC, DMC and DEC with a volume ratio of 1:1:1 were employed as the anode, the separator and the electrolyte, respectively. The junction of the cell was sealed with a rubber gasket to ensure that it was leakproof. The galvanostatic charge/discharge characterization was conducted on a LAND CT3001B battery test system in the voltage range 3.0-4.8 V with a current rate of 0.1C ($1C = 274 \,\mathrm{mAh}\,\mathrm{g}^{-1}$) at room temperature. During the electrochemical process, the in-situ PXRD data were collected on a PANalytical Empyrean diffractometer in the reflection mode (Bragg-Brentano geometry using a CuK α 1 (λ = 1.5406 Å) radiation source) with a flat sample stage and a Ge(111) monochromator at 45 kV and 40 mA. The scan 2θ range was from 15° to 55° with a step size of 0.275° and a total data collection time of 15 min for each round.

cRED and HRTEM characterization. The coin cells with their cathode LCO samples used for TEM characterization were first charged to the designated voltages, and then disassembled in an argon-filled glovebox with water and oxygen content below 0.1 ppm. The charged LCO samples were retrieved by scraping the composite from the cathodes and were washed in NMP to dissolve the binder. The residue solids were later washed in ethanol and deposited on Cu grids for TEM characterization. The cRED datasets for each tested particle were collected on a JEOL-1230 transmission electron microscope operating at an accelerating voltage of 60 kV with a 15-cm camera length, a minimum collection angle of -30° to 30° and a Medipix3 detector. The total number of characterized particles was 50 for N-LCO-P, H-LCO-P, N-LCO-4.5 and H-LCO-4.5, and 20 for the rest of the studied points, with the sample particles randomly chosen. The reciprocal lattice pattern for each raw dataset was then reconstructed and analysed by the REDp software. FIB treatments to obtain suitable slices for simultaneous HRTEM imaging of both the LCO surface and interior were conducted on an FEI Scios DualBeam system. The HRTEM images for the lattice fringes were observed and photographed on a JEOL-3200FS field-emission transmission electron microscope at an accelerating voltage of 300 kV with a OneView CMOS camera (Gatan).

Theoretical calculation methods. To explore the relationship between the lattice length of the *c* axis and the delithiation voltage, an orthorhombic LCO supercell with lattice parameters of 5.67 Å, 4.91 Å and 13.60 Å containing 48 atoms (12 Li, 12 Co and 24 O) was constructed. During the subsequent structural construction for other LCO supercells with curved cobalt oxide layers, the deviated c coordinate of the Co atoms was generated using equation (1), and the coordinates of the Co atoms were fixed while the locations of other atoms, as well as the cell parameters, were first optimized. For the LCO structures with partial delithiation, the interlamellar Li atoms and vacancies were arranged in the six-membered ring to ensure maximum distance between the Li atoms and/or vacancies. The refined LCO structures with different degrees of curvature were thus obtained. The supercell details of typical LCO structures with different degrees of curvature (A = 0, 0.125 and 0.25 Å) are shown in Supplementary Tables 3-5. As for the difference in structural energy, denoted as the local minimum energy of the atomic magnetic moment, it was finally calculated and induced by the different distribution of Co atoms with altered valence due to delithiation. Hence, different initial magnetic moments were also set to obtain the different local minimum energy during the structural optimization process. The force of Co atoms along the c axis and other parameters were also fixed and optimized first. All calculations were performed using Pwmat code, which runs on graphics processing units^{36,37}. SG15 pseudopotentials with 75 Ryd plane wave cut-off energy and density functional theory (DFT) plus U method, with a U value of 3.3 eV for Co d orbitals, were 10. The exchange correlation functionals of Perdew, Burke and Ernzerhof 11 and DFT-D2 van der Waals correction42 were also implemented in all calculations. The number of the K point was set to be $1 \times 5 \times 5$ in the cell with 60 atoms using the Monkhorst-Pack method43. In the relaxations of the flat LCO structure, all atoms and cell parameters were relaxed with the residual force less than 0.01 eV Å-1; in the curved LCO structures, all atoms and cell parameters were also relaxed except the fixed c coordinates of the Co atoms, which were generated following a sine function with their a coordinates. The calculation of the energy cost to lose an oxygen atom was performed with the amplitude of the sine function as 0.3 Å.

Data availability

The data that support the findings of this study are available from the corresponding authors upon reasonable request.

References

- Coelho, A. A. TOPAS and TOPAS-Academic: an optimization program integrating computer algebra and crystallographic objects written in C++. J. Appl. Cryst. 51, 210–218 (2018).
- Jia, W. L. et al. Fast plane wave density functional theory molecular dynamics calculations on multi-GPU machines. J. Comput. Phys. 251, 102–115 (2013).
- Jia, W. L. et al. The analysis of a plane wave pseudopotential density functional theory code on a GPU machine. Comput. Phys. Commun. 184, 9–18 (2013).
- Hamann, D. R. Optimized norm-conserving Vanderbilt pseudopotentials. Phys. Rev. B 88, 1–10 (2013).
- Schlipf, M. & Gygi, F. Optimization algorithm for the generation of ONCV pseudopotentials. Comput. Phys. Commun. 196, 36–44 (2015).
- Cococcioni, M. & de Gironcoli, S. Linear response approach to the calculation of the effective interaction parameters in the LDA+U method. *Phys. Rev. B* 71, 035105 (2005).
- 41. Perdew, J. P., Burke, K. & Ernzerhof, M. Generalized gradient approximation made simple. *Phys. Rev. Lett.* 77, 3865–3868 (1996).
- Grimme, S., Antony, J., Ehrlich, S. & Krieg, H. A consistent and accurate ab initio parametrization of density functional dispersion correction (DFT-D) for the 94 elements H–Pu. *J. Chem. Phys.* 132, 154104 (2010).
- Pack, J. D. & Monkhorst, H. J. "Special points for brillouin-zone integrations"—a reply. *Phys. Rev. B* 16, 1748–1749 (1977).

Acknowledgements

This research is financially supported by the National Key R&D Programme of China (no. 2016YFB0700600), Guangdong Innovative Team Programme (2013N080), Guangdong Key-lab Project (no. 2017B0303010130), Shenzhen Science and Technology Research Grant (no. ZDSYS20170728102618), National Basic Research Programme of China (nos. 2013CB933402 and 2016YFA0301004) and National Natural Science Foundation of China (nos. 21527803, 21621061 and 21871009).

Author contributions

F.P., J.S., K.X. and C.L. conceived the work and designed the experiments. Jianyuan Li, C.L. and W.H. carried out the electrochemical measurements. Jianyuan Li, C.L., P.C. and Y.H. performed the in-situ PXRD experiments. Jianyuan Li and C.L. carried out the cRED and HRTEM characterizations. Y.Q., P.C. and Jian Li assisted with the cRED data analyses. C.L. conducted the FIB treatments. M.W. performed the theoretical calculations. C.L. and W.Z. carried out the SEM and EDS measurements. Jianyuan Li and C.L. performed the XPS measurements. C.L. carried out the ICP-AES experiments. M.Z. collected the synchrotron PXRD data and C.L. carried out the structure refinements. M.Z. and C.D. helped the PXRD analyses. K.Y. performed the DEMS measurements. Z.X. and X.W. helped with the TEM experiments. Jianyuan Li, C.L., K.X., J.S. and F.P. wrote the manuscript. All authors discussed the results and commented on the manuscript.

NATURE NANOTECHNOLOGY ARTICLES

Competing interests

The authors declare no competing interests.

Additional information

Supplementary information The online version contains supplementary material available at https://doi.org/10.1038/s41565-021-00855-x.

Correspondence and requests for materials should be addressed to C.L., K.X., J.S. or E.P.

Peer review information *Nature Nanotechnology* thanks Shi Xue Dou, Michael Toney and the other, anonymous, reviewer(s) for their contribution to the peer review of this work.

Reprints and permissions information is available at www.nature.com/reprints.